In Vivo SPECT Imaging with ^{111}In-DOTA-c(RGDfK) to Detect Early Pancreatic Cancer in a Hamster Pancreatic Carcinogenesis Model

Mitsuyoshi Yoshimoto[1,2], Takuya Hayakawa[1], Michihiro Mutoh[1], Toshio Imai[3], Keisuke Tsuda[2], Sadaaki Kimura[2], Izumi O. Umeda[2], Hirofumi Fujii[2], and Keiji Wakabayashi[1,4]

[1]Cancer Prevention Basic Research Project, National Cancer Center Research Institute, Tokyo, Japan; [2]Functional Imaging Division, National Cancer Center Hospital East, Kashiwa, Japan; and [3]Central Animal Division, National Cancer Center Research Institute, Tokyo, Japan; and [4]Graduate School of Food and Nutritional Sciences, University of Shizuoka, Shizuoka, Japan

Early detection of pancreatic cancer is key to overcoming its poor prognosis. $\alpha_v\beta_3$-integrin is often overexpressed in pancreatic tumor cells, whereas it is scarcely expressed in normal pancreatic cells. In this study, we investigated the usefulness of SPECT imaging with ^{111}In-1,4,7,10-tetraazacylododecane-*N*,*N*′,*N*″,*N*‴-tetraacetic acid-cyclo-(Arg-Gly-Asp-D-Phe-Lys) [^{111}In-DOTA-c(RGDfK)], an imaging probe of $\alpha_v\beta_3$-integrin, for the early detection of pancreatic cancer in a hamster pancreatic carcinogenesis model. **Methods:** Hamsters were subcutaneously injected with the pancreatic duct carcinogen *N*-nitrosobis(2-oxopropyl)amine to induce pancreatic cancer. *N*-nitrosobis(2-oxopropyl)amine–treated hamsters underwent in vivo SPECT with ^{111}In-DOTA-c(RGDfK). After imaging, the tumor-to-normal pancreatic tissue radioactivity ratios in excised pancreatic samples were measured with autoradiography (ARG) and compared with the immunopathologic findings for $\alpha_v\beta_3$-integrin. In a mouse model in which inflammation was induced with turpentine, the uptake of ^{111}In-DOTA-c(RGDfK) in inflammatory regions was evaluated with ARG and compared with that of ^{18}F-FDG. **Results:** ^{111}In-DOTA-c(RGDfK) was clearly visualized in pancreatic cancer lesions as small as 3 mm in diameter. ARG analysis revealed high tumor-to-normal pancreatic tissue radioactivity ratios (4.6 ± 1.0 [mean ± SD] in adenocarcinoma and 3.3 ± 1.4 in atypical hyperplasia). The uptake of ^{111}In-DOTA-c(RGDfK) strongly correlated with $\alpha_v\beta_3$-integrin expression. In the inflammatory model, inflammation-to-muscle ratios for ^{18}F-FDG and ^{111}In-DOTA-c(RGDfK) were 8.37 ± 4.37 and 1.98 ± 0.60, respectively. These results imply that ^{111}In-DOTA-c(RGDfK) has a lower rate of false-positive tumor detection than ^{18}F-FDG. **Conclusion:** Our findings suggest that SPECT with ^{111}In-DOTA-c(RGDfK) has great potential for the early and accurate detection of pancreatic cancer.

Key Words: ^{111}In-DOTA-c(RGDfK); SPECT; $\alpha_v\beta_3$-integrin; pancreatic cancer; early detection

J Nucl Med 2012; 53:765–771
DOI: 10.2967/jnumed.111.099630

Received Oct. 18, 2011; revision accepted Jan. 23, 2012.
For correspondence or reprints contact: Mitsuyoshi Yoshimoto, National Cancer Center Research Institute, 5-1-1 Tsukiji, Chuo-ku, Tokyo 104-0045, Japan.
E-mail: miyoshim@ncc.go.jp
Published online Apr. 10, 2012.

Pancreatic cancer is a leading cause of cancer-related mortality in developed countries, with an increasing incidence (*1*). The 5-y survival rate is poor (*2,3*). Surgical resection remains the only curative option. The postoperative 5-y survival rate has been recorded to be high as 40%–50%, whereas only 15%–20% of tumors are found to be resectable at the time of diagnosis (*4*). Tumor size is an important prognostic factor for pancreatic cancer because better prognosis and postsurgical survival have been reported for small pancreatic cancers (≤2 cm) than for large ones (>2 cm) (*5,6*). Given the incidence and high mortality rate of pancreatic cancer, the development of novel diagnostic technologies is essential for overcoming this type of cancer.

Currently, ^{18}F-FDG PET is widely used in the diagnosis of malignant tumors. ^{18}F-FDG PET is more accurate in detecting relatively large pancreatic adenocarcinomas than conventional imaging techniques (*7–9*). However, it has some limitations in detecting pancreatic cancer (*10*). ^{18}F-FDG can accumulate in chronic and acute pancreatitis, and this fact often yields false-positive interpretations for PET (*11,12*). It is also well known that the sensitivity of ^{18}F-FDG PET in hyperglycemic patients tends to be lower than that in euglycemic patients because elevated serum glucose levels suppress ^{18}F-FDG uptake in tumors by up to 50% as a result of competitive inhibition (*13,14*). New imaging agents that are not influenced by these factors are essential for the detection of small pancreatic cancers.

Integrins are cell adhesion molecules that mediate cell–cell and cell–matrix interactions and contribute to angiogenesis, tumor invasion, and metastasis. $\alpha_v\beta_3$-integrin is a well-characterized integrin that is overexpressed in endothelial cells and various tumor cells (*15–17*). Immunohistochemical analysis demonstrated that $\alpha_v\beta_3$-integrin was expressed in 60% of invasive pancreatic ductal carcinomas of stages I–IV, and patients with $\alpha_v\beta_3$-integrin–positive carcinomas showed shorter survival times than those with $\alpha_v\beta_3$-integrin–negative carcinomas (mean survival times, 12.3 vs. 21.4 mo) (*18*). Thus, $\alpha_v\beta_3$-integrin would be an excellent target for the early detection of malignant pancreatic cancer.

For investigating the mechanisms of the development of pancreatic cancer, an experimental pancreatic ductal carcinogenesis model has been established with the carcinogen *N*-nitrosobis(2-oxopropyl)amine (BOP) in hamsters (*19–22*). This model provides unique characteristics that are similar to a sequence of well-characterized morphologic changes in the human pancreatic duct and frequently shows point mutations in codon 12 of the K-*ras* gene, in accordance with human findings (*23,24*). We found that $\alpha_v\beta_3$-integrin was overexpressed not only in adenocarcinomas but also in atypical hyperplasia in this hamster model (*25*). Therefore, this model is useful in the development of imaging probes for the early detection of pancreatic carcinogenesis.

Radiolabeled Arg-Gly-Asp (RGD) peptides are widely used as $\alpha_v\beta_3$-integrin imaging agents (*26–28*). In a previous study, ^{111}In-1,4,7,10-tetraazacylododecane-*N*,*N*′,*N*″,*N*‴-tetraacetic acid-cyclo-(Arg-Gly-Asp-D-Phe-Lys) [^{111}In-DOTA-c(RGDfK)] showed high uptake in tumors with strong expression of $\alpha_v\beta_3$-integrin, low uptake in normal pancreas, and extremely rapid clearance from the blood (*29*). These characteristics are favorable for pancreatic cancer imaging. In the present study, we investigated the usefulness of SPECT imaging with ^{111}In-DOTA-c(RGDfK) for the early and accurate detection of pancreatic cancer in a chemically induced hamster pancreatic cancer model.

MATERIALS AND METHODS

Experimental Animal Models

Ten 5-wk-old female Syrian golden hamsters were obtained from Japan SLC. For the induction of pancreatic cancer, hamsters were subcutaneously injected with BOP (Nacalai Tesque) in saline at 10 mg/kg of body weight 4 times every other day. Palpation and laparotomy were occasionally performed after BOP treatment to confirm the induction of pancreatic cancer.

Eight 6-wk-old male ddY mice (Japan SLC) were intramuscularly injected with 50 μL of turpentine oil (Kanto Chemical) in the right thigh to induce inflammation (*30,31*).

Animal studies were performed in compliance with the guidelines set for animal experiments by the Committee for Ethics of Animal Experimentation at the National Cancer Center.

SPECT with ^{111}In-DOTA-c(RGDfK) in Hamster Pancreatic Cancer Model

DOTA-c(RGDfK) was labeled with ^{111}In as described previously (*29*). Hamsters were injected via the subclavian vein with 17.5–37.0 MBq of ^{111}In-DOTA-c(RGDfK) 16 wk after treatment with BOP. They were maintained under anesthesia with isoflurane (Dainippon Sumitomo Pharmaceutical) throughout the experiment. Just before the acquisition of CT images, the hamsters were injected with 500 μL of iopamidol (Iopamiron 370; Bayer Schering Pharma).

SPECT/CT was performed with a 4-head, multiplexing, multipinhole NanoSPECT/CT scanner (Bioscan, Inc.) 1 h after the injection of ^{111}In-DOTA-c(RGDfK). First, CT scans were obtained with a tube voltage of 60 kV and a tube current of 0.12 mA. Next, SPECT scanning was performed at 300 s/projection, and 24 projection views were obtained. After imaging, the SPECT data were reconstructed with an ordered-subset expectation maximization algorithm, dedicated software (Invivoscope; Bioscan, Inc.), and Mediso InterViewXP (Mediso). SPECT and CT images were automatically superimposed with Invivoscope. The accuracy of the superimposition was regularly calibrated with phantoms. A researcher experienced in the evaluation of small-animal SPECT/CT images visually evaluated pancreatic uptake.

Autoradiography (ARG) with ^{111}In-DOTA-c(RGDfK) in Hamster Pancreatic Cancer Model

After SPECT/CT, the pancreas from each hamster was excised and macroscopically surveyed to detect pancreatic lesions. Samples were then embedded in Cryo Mount II (Muto Pure Chemicals Co., Ltd.) and frozen in liquid nitrogen. Frozen sections were cut with a cryostat to thicknesses of 20 μm for ARG and 10 μm for histologic analysis and mounted on glass slides. For ARG, glass slides were placed on an imaging plate (BAS-MS 2040; Fujifilm Co. Ltd.), and then the exposed plate was scanned with a bioimaging analyzer (FLA-7000; Fujifilm Co. Ltd.) to detect radioactivity. On the basis

TABLE 1
SPECT Detection Ratios and Tumor-to-Normal Pancreas (T/N) Ratios Calculated by ARG Analysis

Condition	Hamster	Size (mm)	Detection by SPECT	T/N ratio
Adenocarcinoma	4	2.0	ND	5.1
	5	3.0	Detected	4.0
		4.4	Detected	5.2
	6	3.0	Detected	4.5
		5.0	Detected	6.7
	7	2.0	ND	4.5
	9	3.5	ND	3.5
		5.0	Detected	4.2
	10	8.0	Detected	3.7
Atypical hyperplasia	3	1.5	ND	4.9
	7	0.7	ND	5.4
	9	0.8	ND	2.6
		1.3	ND	2.7
	10	0.9	ND	2.4

For adenocarcinoma and atypical hyperplasia, respective sizes (mean ± SD) were 4.0 ± 1.9 and 1.0 ± 0.3 mm; respective percentages detected by SPECT were 66.7% and 0%; and respective T/N ratios (mean ± SD) were 4.6 ± 1.0 and 3.9 ± 1.5. ND = not detected.

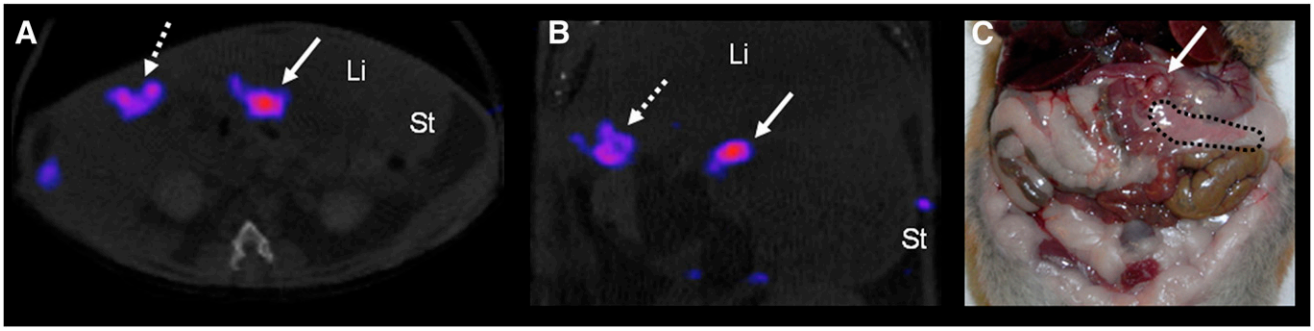

FIGURE 1. (A and B) SPECT images of pancreatic tumor in hamster 6 (A, axial; B, coronal). SPECT was performed 1 h after injection of ^{111}In-DOTA-c(RGDfK). Intense uptake was found in tumor (solid arrow). Slight uptake of ^{111}In-DOTA-c(RGDfK) was observed in intestine (dotted arrow). (C) Anatomic image of hamster abdomen. Tumor (5 mm) in pancreatic head is indicated by arrow; its position was identical to that of region of high uptake of ^{111}In-DOTA-c(RGDfK). Pancreatic gastric lobe is indicated by dotted line. Li = liver; St = stomach.

of microscopic observation of sections stained with hematoxylin and eosin, regions of interest were placed on both tumor and normal pancreatic samples. ImageQuant software (Fujifilm Co. Ltd.) was used to quantify the intensity of radioactivity.

ARG with ^{111}In-DOTA-c(RGDfK) and ^{18}F-FDG in Mouse Inflammatory Model

Three days after turpentine oil injection, ARG analysis of inflammatory regions was performed. Eight mice were divided into 2 groups. Each group was injected via the tail vein with 740 kBq of ^{111}In-DOTA-c(RGDfK) and 925 kBq of ^{18}F-FDG. Inflammatory tissue, including the surrounding tissue, was excised 1 h after injection. ARG analysis was performed as described earlier. Regions of interest were placed on both inflammatory and muscle regions.

Immunohistochemical Analysis of $\alpha_v\beta_3$-Integrin

Frozen sections (10 μm) were fixed in methanol at −20°C. After 2 washes with phosphate-buffered saline containing 0.05% polysorbate 20 (PBS-T), endogenous peroxide was blocked with 3% H_2O_2 in methanol for 10 min. After 2 washes with PBS-T, sections were masked with 2% normal goat serum in PBS-T for 1 h at room temperature and then incubated overnight with anti–$\alpha_v\beta_3$-integrin (clone LM609; Millipore) at 4°C. Sections were incubated with biotinylated anti–mouse IgG (Dako Cytomation); this step was followed by reaction with streptavidin–biotin–horseradish peroxidase complex (StreptABComplex/HRP; Dako Cytomation). Horseradish peroxidase was detected with diaminobenzidine (Phoenix Biotechnologies) substrate. All sections were counterstained with hematoxylin.

Statistical Analysis

Data analysis was performed with GraphPad Prism (GraphPad Software). Unpaired t testing was used for ARG analysis in the mouse inflammatory model. The results were considered statistically significant at $P < 0.05$.

RESULTS

SPECT with ^{111}In-DOTA-c(RGDfK) in BOP-Treated Hamsters

Adenocarcinomas or atypical pancreatic hyperplasia was macroscopically or microscopically found in 7 of 10 BOP-treated hamsters (Supplemental Table 1) (supplemental materials are available online only at http://jnm.snmjournals.org). There were 9 adenocarcinoma lesions in 6 BOP-treated hamsters and 5 atypical hyperplasia lesions in 4 BOP-treated hamsters. Both adenocarcinomas and atypical hyperplasia were observed in 3 BOP-treated hamsters. The average size (mean ± SD) of the adenocarcinomas was 4.0 ± 1.9 mm, and SPECT with ^{111}In-DOTA-c(RGDfK) detected 6 of the 9 lesions (66.7%) (Table 1). The average size of the atypical hyperplasia lesions was 1.0 ± 0.3 mm, and SPECT with ^{111}In-DOTA-c(RGDfK) could not detect any such lesion.

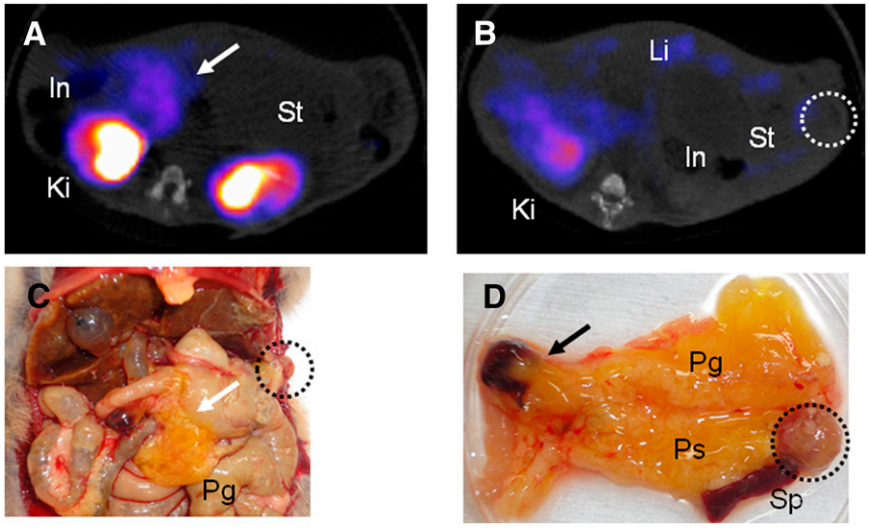

FIGURE 2. (A and B) SPECT axial images of pancreatic tumor (A) and purulent inflammatory lesion (B) in hamster 10. (C and D) Anatomic images of abdomen (C) and excised pancreas (D). Tumor (8 mm) in pancreatic head is indicated by arrow. Inflammatory lesion is indicated by dotted circle. In = intestine; Ki = kidney; Li = liver; Pg = pancreatic gastric lobe; Ps = pancreatic splenic lobe; Sp = spleen; St = stomach.

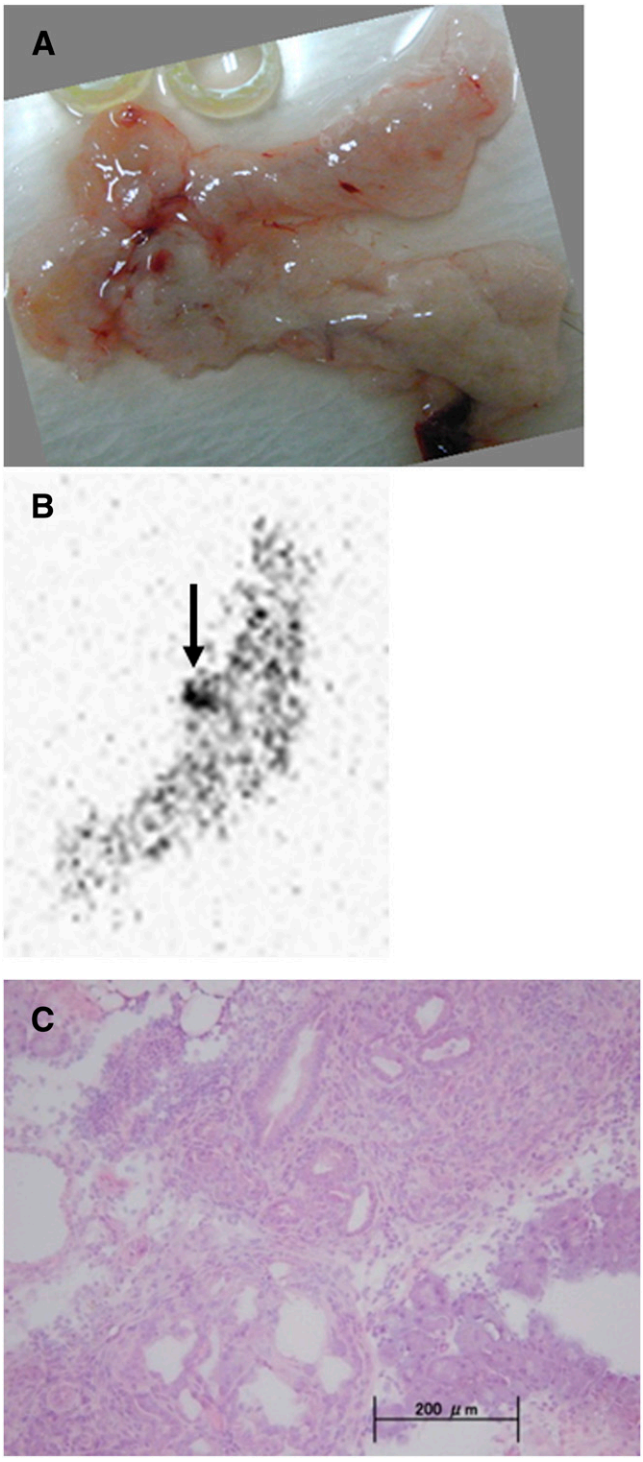

FIGURE 3. Ex vivo autoradiography and histopathologic analysis of atypical hyperplastic region in hamster 3. (A) Macroscopically, there was no lesion in pancreas. (B) One hot spot (arrow) was found in gastric lobe by ARG, but SPECT could not detect this small lesion. (C) Hematoxylin–eosin staining in region of hot spot.

Abdominal CT images of hamsters successfully depicted the liver, stomach, intestine, and kidneys. The anatomic relationships among these organs successfully indicated the location of the pancreas, although the actual pancreatic contours were not delineated. Because SPECT images were accurately superimposed on CT images, pathologic accumulation in the pancreas could be judged from the SPECT/CT fusion images. Representative SPECT/CT fusion images are shown in Figure 1 and Figure 2. Figures 1A and 1B show SPECT images of the pancreatic tumor in hamster 6. A tumor that was 5 mm in diameter and that was located near the pyloric region was clearly visualized with ^{111}In-DOTA-c(RGDfK). Although there was slight uptake in the intestine, this kind of uptake never interfered with the detection of pancreatic tumors because superimposed CT images clearly indicated that the uptake was not located in the pancreas. All tumors depicted by ^{111}In-DOTA-c(RGDfK) SPECT were verified by laparotomy findings (Figs. 1B and 1C).

In hamster 10, 1 pancreatic tumor (8 mm in diameter) in the pancreatic head and an artificially induced purulent inflammatory/foreign-body granulomatous nodule that was located in the splenic lobe of the pancreas and that was adherent to abdominal muscle were found (Figs. 2C and 2D, Ps). SPECT with ^{111}In-DOTA-c(RGDfK) accurately depicted the tumor in the pancreatic head (Fig. 2A),but the inflammatory lesion was not detected (Figs. 2B and 2D). There was intense uptake in the kidneys because of urinary excretion.

Ex Vivo ARG and Histopathologic Analysis of Excised Pancreas

ARG successfully depicted all adenocarcinoma and atypical hyperplasia lesions, but SPECT failed to detect atypical hyperplasia. The T/N ratios for adenocarcinomas and atypical hyperplasia were 4.6 ± 1.0 and 3.9 ± 1.5, respectively (Table 1). There was strong $\alpha_v\beta_3$-integrin expression in all adenocarcinoma lesions.

The contrast in ^{111}In-DOTA-c(RGDfK) accumulation on ARG images between tumors and the normal pancreas was quite good (Supplemental Figs. 1A and 1B). Strong positive results for $\alpha_v\beta_3$-integrin in tumor tissues on immunohistochemical analysis validated these results satisfactorily (Supplemental Fig. 1C).

Although SPECT failed to detect atypical hyperplasia lesions, ARG successfully depicted all of them, even when they were not macroscopically visualized. In hamster 3 (Fig. 3), the T/N ratio was 4.9—similar to that for adenocarcinoma (4.6). However, SPECT could not detect this lesion, likely because of its small size.

In hamster 10, the uptake of ^{111}In-DOTA-c(RGDfK) in the inflammatory lesion was not demonstrated even by ARG (Supplemental Fig. 2). In agreement with the in vivo SPECT findings (Fig. 2), ARG images revealed significant uptake of ^{111}In-DOTA-c(RGDfK) in tumors but not in inflammatory lesions. The T/N ratio was 3.7, and the ratio of inflammation to the normal pancreas was 0.9. These accumulation patterns were verified by the absence of $\alpha_v\beta_3$-integrin expression in inflammatory lesions.

Accumulation of ^{111}In-DOTA-c(RGDfK) and ^{18}F-FDG in Inflammatory Lesions

The uptake of ^{111}In-DOTA-c(RGDfK) was compared with that of ^{18}F-FDG in inflammatory lesions in the mouse

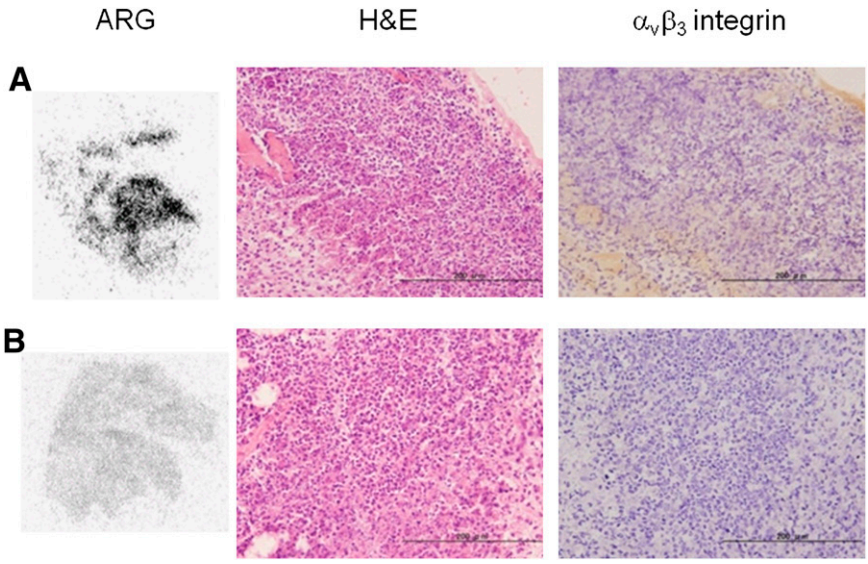

FIGURE 4. Ex vivo autoradiography [A, ^{18}F-FDG; B, ^{111}In-DOTA-c(RGDfK)] and histopathologic analysis of inflammation induced by turpentine oil in mouse model. Sections of inflammatory regions were stained with hematoxylin–eosin (H&E) and anti–$\alpha_v\beta_3$-integrin antibody.

model (Fig. 4 and Fig. 5). In this model, acute inflammation was characterized by focal neutrophil infiltration (Fig. 4). Although ^{18}F-FDG was actively taken up in the inflammatory regions in all cases, ^{111}In-DOTA-c(RGDfK) was not. There was no expression of $\alpha_v\beta_3$-integrin in this inflammatory model. The inflammation-to-muscle ratio for ^{18}F-FDG was much higher than that for ^{111}In-DOTA-c(RGDfK) (8.37 ± 4.37 vs. 1.98 ± 0.60; $P < 0.05$) (Fig. 5).

DISCUSSION

Because $\alpha_v\beta_3$-integrin is often expressed in various kinds of malignant tumors and endothelial cells, tumor imaging with radiolabeled RGD peptides, which are promising agents for $\alpha_v\beta_3$-integrin imaging, has been actively investigated in animal models and cancer patients (*26–29*). Haubner et al. showed that there was a correlation between the tumor uptake of ^{18}F-galacto-c(RGDfK) and the level of $\alpha_v\beta_3$-integrin expression (*27*). We developed ^{111}In-DOTA-c(RGDfK), an ^{111}In-labeled RGD, and demonstrated that this radiopharmaceutical showed high tumor uptake in SKOV-3, a human ovarian carcinoma model, with strong expression of $\alpha_v\beta_3$-integrin (*29*).

Pancreatic cancer, one of the most incurable malignant tumors, can also be imaged with radiolabeled RGD peptides because pancreatic cancer cells express $\alpha_v\beta_3$-integrin (*18*). However, successful cure of pancreatic cancer requires detection in the early stages of carcinogenesis, when the lesions are small. For this purpose, suitable animal models that mimic the clinical situation as closely as possible are ideal tools. The hamster model used in the present study is well established and has been used for numerous studies of pancreatic duct carcinogenesis and its prevention (*20,32,33*). Because this carcinogenesis model appeared to be suitable for evaluation of the usefulness of imaging agents in the early detection of pancreatic cancer, we investigated the possibility of early and accurate detection of this cancer by combining this model and SPECT with ^{111}In-DOTA-c(RGDfK).

In the present study, SPECT with ^{111}In-DOTA-c(RGDfK) clearly demonstrated 66.7% of pancreatic adenocarcinomas in the hamster model. The smallest pancreatic adenocarcinoma detected was 3 mm. This encouraging finding regarding the detection of early pancreatic cancer was validated by the high T/N ratio, as shown by ARG. This good contrast between tumors and normal tissues may be explained by the fact that $\alpha_v\beta_3$-integrin is strongly expressed in adenocarcinoma lesions but not in stroma and normal ductal cells. Our histopathologic examination reconfirmed this finding. The results of the present study demonstrated that our strategy of using $\alpha_v\beta_3$-integrin as a molecular target was entirely appropriate. Especially important was the fact that SPECT yielded no false-positive findings in normal pancreatic tissue.

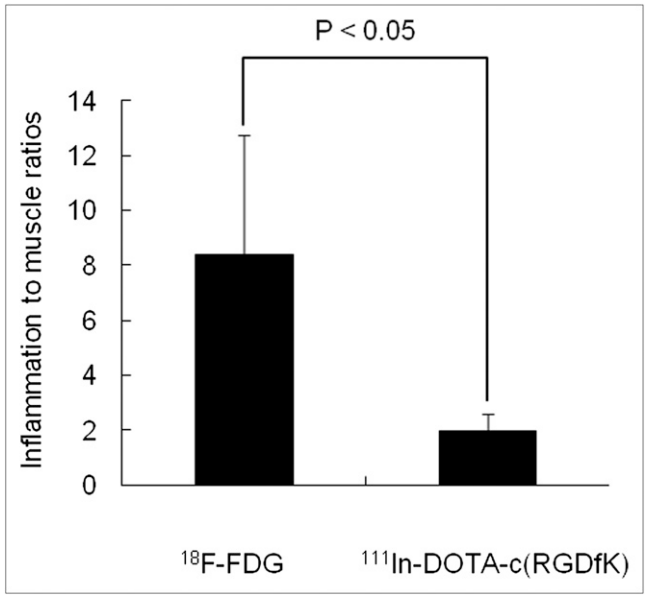

FIGURE 5. Ratios of inflammation to muscle for ^{18}F-FDG and ^{111}In-DOTA-c(RGDfK), as calculated by ARG analysis ($n = 4$).

ARG analysis demonstrated positive uptake in atypical hyperplasia, but SPECT did not. One reason for this difference could be lesion size. The average size of atypical hyperplasia lesions is 1.0 mm—too small for detection by in vivo SPECT. Another reason could be that the uptake of ^{111}In-DOTA-c(RGDfK) in atypical hyperplasia was relatively lower than that in adenocarcinomas; however, this reason suggests that $\alpha_v\beta_3$-integrin would be a good target for the early detection of pancreatic cancer with radiolabeled RGD peptides because atypical hyperplasia lesions can be regarded as precancerous lesions in terms of carcinogenesis.

In the clinical application of SPECT with ^{111}In-DOTA-c(RGDfK), it is important to clarify the anatomic location of the radionuclide uptake. In the present study, we used a SPECT/CT combination scanner, although this scanner was dedicated to small-animal imaging. Through SPECT/CT fusion imaging, we identified the pancreas on the basis of the location of the kidneys, liver, intestine, and stomach, which are relatively clearly visualized on CT. SPECT/CT combination scanners are becoming popular in clinical practice. Because the performance of clinical CT scanners is better than that of small-animal units with regard to acquisition time, tube voltage, and current × time product (mAs), identification of the pancreas would be easier in clinical practice. Fusion imaging with MRI and scintigraphy is now actively under investigation. Current high-magnetic-field MRI scanners can provide high-resolution anatomic images without contrast agents. Therefore, fusion imaging with MRI and PET or SPECT would overcome the concern about identification of the pancreas (*34*).

^{18}F-FDG PET may have become more popular for the detection of malignant tumors, but ^{18}F-FDG also has a high affinity for inflammatory lesions, resulting in false-positive findings. Because pancreatic masses or swellings are sometimes caused by inflammatory changes, ^{18}F-FDG PET may produce false-positive results. To examine whether SPECT with ^{111}In-DOTA-c(RGDfK) is more useful than ^{18}F-FDG PET in the differentiation of inflammatory lesions, we compared the uptake of ^{111}In-DOTA-c(RGDfK) in inflammatory lesions induced by turpentine in a mouse inflammatory model with the uptake of ^{18}F-FDG. The uptake of ^{111}In-DOTA-c(RGDfK) in inflammatory lesions and the expression of $\alpha_v\beta_3$-integrin were not found, resulting in a significantly lower inflammation-to-muscle ratio for ^{111}In-DOTA-c(RGDfK) than for ^{18}F-FDG. In contrast, ARG indicated high ^{18}F-FDG uptake in inflammatory lesions, in agreement with a previous report (*31*). This profile of $\alpha_v\beta_3$-integrin expression is favorable for distinguishing between tumors and inflammation. In pancreatic lesions, false-positive results for the detection of cancer may be harmful because pancreatic biopsy is somewhat invasive. Therefore, ^{111}In-DOTA-c(RGDfK) may be superior to ^{18}F-FDG for the early and accurate detection of pancreatic cancer.

CONCLUSION

The results of the present study indicated that SPECT with ^{111}In-DOTA-c(RGDfK) is a powerful tool for the diagnosis of pancreatic cancer in the hamster carcinogenesis model, even though a limitation was imposed by the small number of animals evaluated. The specific uptake of ^{111}In-DOTA-c(RGDfK) in tumors and not in inflammatory lesions could decrease the incidence of false-positive findings. Our results will promote the clinical application of ^{111}In-DOTA-c(RGDfK) and other $\alpha_v\beta_3$-integrin imaging agents in the diagnosis of pancreatic cancer.

DISCLOSURE STATEMENT

The costs of publication of this article were defrayed in part by the payment of page charges. Therefore, and solely to indicate this fact, this article is hereby marked "advertisement" in accordance with 18 USC section 1734.

ACKNOWLEDGMENTS

This work was supported in part by a Grant-in-Aid for Exploratory Research and a Grant-in-Aid for Young Scientists (B) from the Ministry of Education, Culture, Sports, Science, and Technology. No other potential conflict of interest relevant to this article was reported.

REFERENCES

1. Qiu D, Katanoda K, Marugame T, Sobue T. A Joinpoint regression analysis of long-term trends in cancer mortality in Japan (1958-2004). *Int J Cancer.* 2009;124:443–448.
2. Jemal A, Siegel R, Xu J, Ward E. Cancer statistics, 2010. *CA Cancer J Clin.* 2010;60:277–300.
3. Tsukuma H, Ajiki W, Ioka A, Oshima A. Survival of cancer patients diagnosed between 1993 and 1996: a collaborative study of population-based cancer registries in Japan. *Jpn J Clin Oncol.* 2006;36:602–607.
4. Li D, Xie K, Wolff R, Abbruzzese JL. Pancreatic cancer. *Lancet.* 2004;363:1049–1057.
5. Pongprasobchai S, Pannala R, Smyrk TC, et al. Long-term survival and prognostic indicators in small (≤2 cm) pancreatic cancer. *Pancreatology.* 2008;8:587–592.
6. Agarwal B, Correa AM, Ho L. Survival in pancreatic carcinoma based on tumor size. *Pancreas.* 2008;36:e15–e20.
7. Kauhanen SP, Komar G, Seppanen MP, et al. A prospective diagnostic accuracy study of ^{18}F-fluorodeoxyglucose positron emission tomography/computed tomography, multidetector row computed tomography, and magnetic resonance imaging in primary diagnosis and staging of pancreatic cancer. *Ann Surg.* 2009;250:957–963.
8. Sendler A, Avril N, Helmberger H, et al. Preoperative evaluation of pancreatic masses with positron emission tomography using ^{18}F-fluorodeoxyglucose: diagnostic limitations. *World J Surg.* 2000;24:1121–1129.
9. Okano K, Kakinoki K, Akamoto S, et al. ^{18}F-fluorodeoxyglucose positron emission tomography in the diagnosis of small pancreatic cancer. *World J Gastroenterol.* 2011;17:231–235.
10. Delbeke D, Pinson CW. Pancreatic tumors: role of imaging in the diagnosis, staging, and treatment. *J Hepatobiliary Pancreat Surg.* 2004;11:4–10.
11. Diederichs CG, Staib L, Vogel J, et al. Values and limitations of ^{18}F-fluorodeoxyglucose-positron-emission tomography with preoperative evaluation of patients with pancreatic masses. *Pancreas.* 2000;20:109–116.
12. Shreve PD. Focal fluorine-18 fluorodeoxyglucose accumulation in inflammatory pancreatic disease. *Eur J Nucl Med.* 1998;25:259–264.
13. Delbeke D, Rose DM, Chapman WC, et al. Optimal interpretation of FDG PET in the diagnosis, staging, and management of pancreatic carcinoma. *J Nucl Med.* 1999;40:1784–1791.
14. Diederichs CG, Staib L, Glatting G, Beger HG, Reske SN. FDG PET: elevated plasma glucose reduces both uptake and detection rate of pancreatic malignancies. *J Nucl Med.* 1998;39:1030–1033.
15. Brooks PC. Role of integrins in angiogenesis. *Eur J Cancer.* 1996;32A:2423–2429.
16. Brooks PC, Clark RA, Cheresh DA. Requirement of vascular integrin $\alpha_v\beta_3$ for angiogenesis. *Science.* 1994;264:569–571.
17. Mizejewski GJ. Role of integrins in cancer: survey of expression patterns. *Proc Soc Exp Biol Med.* 1999;222:124–138.

18. Hosotani R, Kawaguchi M, Masui T, et al. Expression of integrin $\alpha_v\beta_3$ in pancreatic carcinoma: relation to MMP-2 activation and lymph node metastasis. *Pancreas.* 2002;25:e30–e35.
19. Mizumoto K, Tsutsumi M, Denda A, Konishi Y. Rapid production of pancreatic carcinoma by initiation with *N*-nitroso-bis(2-oxopropyl)amine and repeated augmentation pressure in hamsters. *J Natl Cancer Inst.* 1988;80:1564–1567.
20. Takahashi M, Kitahashi T, Ishigamori R, et al. Increased expression of inducible nitric oxide synthase (iNOS) in *N*-nitrosobis(2-oxopropyl)amine-induced hamster pancreatic carcinogenesis and prevention of cancer development by ONO-1714, an iNOS inhibitor. *Carcinogenesis.* 2008;29:1608–1613.
21. Nishikawa A, Furukawa F, Imazawa T, Yoshimura H, Mitsumori K, Takahashi M. Effects of caffeine, nicotine, ethanol and sodium selenite on pancreatic carcinogenesis in hamsters after initiation with *N*-nitrosobis(2-oxopropyl)amine. *Carcinogenesis.* 1992;13:1379–1382.
22. Pour P, Althoff J, Kruger FW, Mohr U. A potent pancreatic carcinogen in Syrian hamsters: *N*-nitrosobis(2-oxopropyl)amine. *J Natl Cancer Inst.* 1977;58:1449–1453.
23. Fujii H, Egami H, Chaney W, Pour P, Pelling J. Pancreatic ductal adenocarcinomas induced in Syrian hamsters by *N*-nitrosobis(2-oxopropyl)amine contain a c-Ki-ras oncogene with a point-mutated codon 12. *Mol Carcinog.* 1990;3:296–301.
24. Tsutsumi M, Kondoh S, Noguchi O, et al. K-ras gene mutation in early ductal lesions induced in a rapid production model for pancreatic carcinomas in Syrian hamsters. *Jpn J Cancer Res.* 1993;84:1101–1105.
25. Kitahashi T, Yoshimoto M, Imai T. Novel immunohistochemical marker, integrin $\alpha_v\beta_3$, for BOP-induced early lesions in hamster pancreatic ductal carcinogenesis. *Oncol Lett.* 2011;2:229–234.
26. Beer AJ, Schwaiger M. Imaging of integrin $\alpha_v\beta_3$ expression. *Cancer Metastasis Rev.* 2008;27:631–644.
27. Haubner R, Weber WA, Beer AJ, et al. Noninvasive visualization of the activated $\alpha_v\beta_3$ integrin in cancer patients by positron emission tomography and [^{18}F]galacto-RGD. *PLoS Med.* 2005;2:e70.
28. Haubner R, Wester HJ, Weber WA, et al. Noninvasive imaging of $\alpha_v\beta_3$ integrin expression using ^{18}F-labeled RGD-containing glycopeptide and positron emission tomography. *Cancer Res.* 2001;61:1781–1785.
29. Yoshimoto M, Ogawa K, Washiyama K, et al. $\alpha_v\beta_3$ Integrin-targeting radionuclide therapy and imaging with monomeric RGD peptide. *Int J Cancer.* 2008; 123:709–715.
30. Liu RS, Chou TK, Chang CH, et al. Biodistribution, pharmacokinetics and PET imaging of [^{18}F]FMISO, [^{18}F]FDG and [^{18}F]FAc in a sarcoma- and inflammation-bearing mouse model. *Nucl Med Biol.* 2009;36:305–312.
31. Yamada S, Kubota K, Kubota R, Ido T, Tamahashi N. High accumulation of fluorine-18-fluorodeoxyglucose in turpentine-induced inflammatory tissue. *J Nucl Med.* 1995;36:1301–1306.
32. Nishikawa A, Furukawa F, Lee IS, Tanaka T, Hirose M. Potent chemopreventive agents against pancreatic cancer. *Curr Cancer Drug Targets.* 2004;4:373–384.
33. Takeuchi Y, Takahashi M, Sakano K, et al. Suppression of *N*-nitrosobis(2-oxopropyl) amine-induced pancreatic carcinogenesis in hamsters by pioglitazone, a ligand of peroxisome proliferator-activated receptor gamma. *Carcinogenesis.* 2007;28:1692–1696.
34. Tatsumi M, Isohashi K, Onishi H, et al. ^{18}F-FDG PET/MRI fusion in characterizing pancreatic tumors: comparison to PET/CT. *Int J Clin Oncol.* 2011;16:408–415.

JNM The Journal of NUCLEAR MEDICINE

In Vivo SPECT Imaging with ^{111}In-DOTA-c(RGDfK) to Detect Early Pancreatic Cancer in a Hamster Pancreatic Carcinogenesis Model

Mitsuyoshi Yoshimoto, Takuya Hayakawa, Michihiro Mutoh, Toshio Imai, Keisuke Tsuda, Sadaaki Kimura, Izumi O. Umeda, Hirofumi Fujii and Keiji Wakabayashi

J Nucl Med. 2012;53:765-771.
Published online: April 10, 2012.
Doi: 10.2967/jnumed.111.099630

The Journal of Nuclear Medicine is published monthly.
SNMMI | Society of Nuclear Medicine and Molecular Imaging
1850 Samuel Morse Drive, Reston, VA 20190.
(Print ISSN: 0161-5505, Online ISSN: 2159-662X)

SNMMI SOCIETY OF NUCLEAR MEDICINE AND MOLECULAR IMAGING